Available online at www.sciencedirect.com
ScienceDirect
Ceramics International 37 (2011) 443–449
CERAMICS INTERNATIONAL
www.elsevier.com/locate/ceramint

Synthesis of Fe–TiC–Al_2O_3 hybrid nanocomposite via carbothermal reduction enhanced by mechanical activation

Mansour Razavi [a,*], Amir Hossein Rajabi-Zamani [a], Mohammad Reza Rahimipour [a], Reza Kaboli [b], Mohsen Ostad Shabani [a,c], Rahim Yazdani-Rad [a]

[a] Department of Ceramic, Materials and Energy Research Center (MERC), P.O. Box 14155-4777, Tehran, Iran
[b] Department of Metallurgy, Clausthal University of Technology, Robert-Koch-Str. 42, 38678 Clausthal-Zellerfeld, Germany
[c] Department of Materials Science and Engineering, Sharif University of Technology (SUT), P.O. Box 11365-9466, Tehran, Iran

Received 9 February 2010; received in revised form 6 August 2010; accepted 2 September 2010
Available online 29 September 2010

Abstract

In this study, the feasibility of the synthesis of Fe–TiC–Al_2O_3 hybrid nanocomposite via mechanical activation followed by carbothermal reduction was investigated. The raw materials including ilmenite, carbon black and aluminum powder were milled in a high energy planetary ball mill. At different time intervals, samples were taken for characterization. After phase evaluation with XRD, some samples were heat treated in an atmosphere controlled tube furnace. Studies proved that increasing the milling time of the raw materials resulted in the formation of more amorphous phase and more active materials. Furthermore, investigations showed that after carbothermal reduction, the synthesized TiC crystallites were in the scale of nanometers and the lattice parameter had some deviation from the standard value. At higher heat treatment temperatures, the crystallite sizes increased, while the deviation from the standard lattice parameter decreased.

Keywords: Hybrid nanocomposite; Mechanical activation; Titanium carbide; Ilmenite

1. Introduction

The existence of hard ceramics in the rather soft metallic matrix has made metal matrix composites (MMCs) interesting materials [1,2]. Among MMCs, despite high density, ferrous matrix composites are still desirable due to easy and inexpensive production in addition to more isotropic properties [3]. The properties of a composite are determined by the characteristics of the reinforcing phase and also the compatibility of this phase with the matrix. Consequently, the production of a hybrid composite including a combination of several types of reinforcing materials can result in unique mechanical and wear properties [4–7]. Among common reinforcing phases, TiC with the crystal structure of NaCl is desirable due to its high hardness, low density, high melting point, high elastic modulus, excellent wear and corrosion resistance, proper electrical conductivity, high thermal shock resistance, good wettability and stability in iron melt [8–12].

These composites can be produced via different methods including HP, HIP, SHS and infiltration. Using common methods often result in the production of big agglomerates obstructing the distribution of the secondary phase in the matrix. Additionally, long time periods and high temperatures of these methods cause the appearance of large crystallites. Mechanical synthesis activation (MSA), which is nowadays used for the production of a wide range of nanocrystalline compositions and amorphous phases, reduces the time and temperature of the reaction as well as increasing the production rate, in comparison with common routes. In this method, during milling process, a portion of the energy of the ball mill is transferred to the powder causing reduction in the crystallite sizes in addition to increase in the crystal defects including dislocations, structural distortion and atom displacement. All the above bring about more activation of the material, which can greatly stimulate the kinetics of the reaction [13–17]. Several researchers have taken advantage of this method to raise the speed of leaching, thermal processes

* Corresponding author. Tel.: +98 261 6204131; fax: +98 261 6201888.
E-mail addresses: m-razavi@merc.ac.ir, m7816006@yahoo.com (M. Razavi).

0272-8842/$36.00
doi:10.1016/j.ceramint.2010.09.013

Table 1
Chemical analysis of the used ilmenite concentrate.

Element	TiO_2	FeO	Fe_2O_3	Al_2O_3	MnO	MgO	SiO_2	CaO	V_2O_5	Cr_2O_3	P_2O_5	Other
Weight percent	47.40	34.20	10.60	1.30	1.70	1.00	2.00	1.00	0.30	0.03	0.15	Balance

and carbothermal reduction of minerals [18]. Final properties of the materials synthesized through this method are highly dependent upon the mechanical, physical and chemical characteristics of the raw materials and also the milling parameters such as the rotational speed, milling time, milling type, and atmosphere [15–19]. Pursuing previous studies [20], the feasibility of the synthesis of Fe–TiC–Al_2O_3 hybrid nanocomposite via mechanical activation plus subsequent carbothermal reduction was investigated.

2. Experimental

In this research, three types of raw materials were used: ilmenite with the particle size of <150 mesh from Kahnouj mine in Iran with the chemical analysis illustrated in Table 1, amorphous carbon black with the particle size of <250 mesh and aluminum powder with the purity of 99.99% and the particle size of <250 mesh. The mentioned raw materials with the stoichiometric ratio of Eq. (1) including 10 wt.% of aluminum were mixed in a high energy planetary mill and sampled after different time intervals. From thermodynamic calculations and also previous researches [20,21], it seems that 10 wt.% of aluminum is sufficient to reduction of ilmenite:

$$FeTiO_3 + 4C = Fe + TiC + 3CO \quad (1)$$

The rotational speed of the disc and the cup were 410 and 700 rpm, respectively. The cup and the balls were made of high chrome stainless steel with the diameters of 70 and 20 mm, respectively. There were 3 balls and the ball to powder ratio (BPR) was 1:10. Also, in order to protect the materials against oxidation and to prevent unexpected reactions, argon with the purity of 99.9999% and the pressure of 2.5 bars was employed in the filled cup. To accomplish the reactions and also to study the influence of the activation of materials on the reaction temperature, heat treatment was performed in an atmosphere

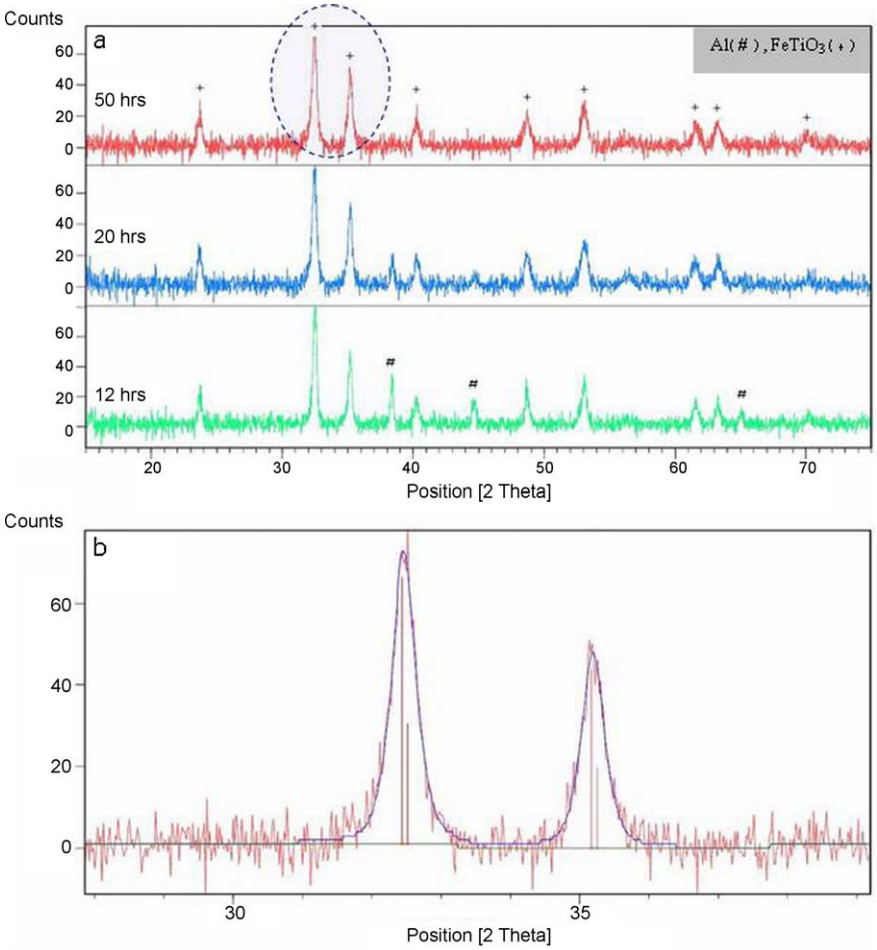

Fig. 1. (a) The XRD pattern of the samples milled for different time periods. (b) Fitted curve of the highlighted area of the XRD pattern above ($\gamma = 0.68$).

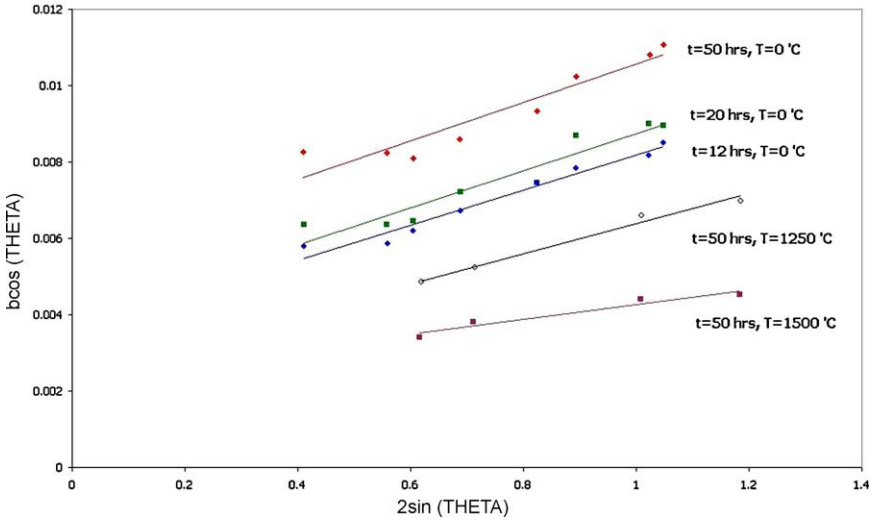

Fig. 2. Williamson–Hall diagram for the calculation of the crystallite sizes and the mean strain.

controlled tube furnace. Tablet samples were prepared with the diameter and thickness of 20 and 5 mm, respectively. Subsequently, the samples were heat treated in the mentioned furnace under argon atmosphere with the discharge of 1.9–2.2 l/min. To detect the produced phases and compositions and also to calculate the crystallite size and lattice parameter, XRD was utilized with the voltage of 30 kV, the current of 25 mA and Cu Kα with the wavelength of 1.5405 Å. Williamson–Hall method was used to determine the crystallite size and the mean strain in the crystals. To calculate the lattice parameter, Nelson–Riley method was used [22]. To measure the full-width at half-maximum (FWHM), PANalytical X'Pert HighScore software was operated. X'Pert HighScore uses the Pseudo-Voigt profile function, which is the weighted mean between a Lorentz and a Gauss function:

$$G_{ik} = \gamma \frac{C_0^{1/2}}{H_k \pi} [1 + C_0 X_{ik}^2]^{-1} + (1-\gamma) \frac{C_1^{1/2}}{H_k \pi^{1/2}} \exp[-C_1 X_{ik}^2] \quad (2)$$

where $C_0 = 4$, $C_1 = 4 \times \ln 2$, H_k is FWHM of the kth Bragg reflection, $X_{ik} = (2\theta_i - 2\theta_k)/H_k\gamma$ is a refinable mixing parameter describing the amount of Gaussian profile versus the amount of Lorentzian profile; and thus describing the overall profile shape. Inductively coupled plasma (ICP) and combustion methods were used to determine the metallic elements and carbon content, respectively. Finally, the consolidated densities of materials were determined by Archimedes' principle using water immersion.

Table 2
The mean crystallite size and mean strain according to Williamson–Hall equation (where d equals the crystallite size, η is the mean strain).

Milling time (h)	Temperature of heat treatment (°C)	$y = ax + b$		d (nm)	η (%)
		a	b		
12	0	0.0046	0.0036	38.51	0.46
20	0	0.0049	0.0039	35.55	0.49
50	0	0.0051	0.0055	25.21	0.51
50	1250	0.0039	0.0025	55.46	0.39
50	1500	0.0019	0.0023	60.28	0.19

3. Results and discussion

X-ray diffraction patterns of the samples milled for 12, 20 and 50 h are illustrated in Fig. 1. As observed, milling did not have a specific impact on the phases. After all time periods, Al and $FeTiO_3$ are the only phases detected in the powders. The only change occurred after longer milling times is the broadening and the slight fall of the peaks, which can be attributed to the decrease in the size of ilmenite crystallites.

Since the amount of amorphization during milling can be an indicator of material activation, the following equation introduced by Ohlberg and Strickler can be used to determine the amount of the amorphous phase [23]:

$$Y = 100 - X = 100 - \left(\frac{U_n}{I_n} \times \frac{I_a}{U_a} \times 100 \right) \quad (3)$$

where U and I are the background and the integral intensities of different peaks, respectively. Y is the portion of the amorphous phase and X is the portion of the crystalline phase. Also, n and a are the indexes representing the non-activated and activated samples. To determine the amorphization degree, it is assumed that the sample milled for 12 h is not activated and has no amorphous phase. With this assumption and with the use of the eight peaks of ilmenite, the amorphization degrees for the samples milled for 20 and 50 h are 14.44 and 16.82%, respectively. In Fig. 2, Williamson–Hall diagram is illustrated for the calculation of the crystallite size and the strain in the system. The calculation results are also presented in Table 2. According to Table 2, as predicted, increasing the milling time resulted in the decrease in the crystallite sizes of ilmenite so that after 50 h of milling the crystallite size decreased to 25 nm. Moreover, increasing the milling time caused an increase in the mean strain in the crystals. Therefore, when the milling time is

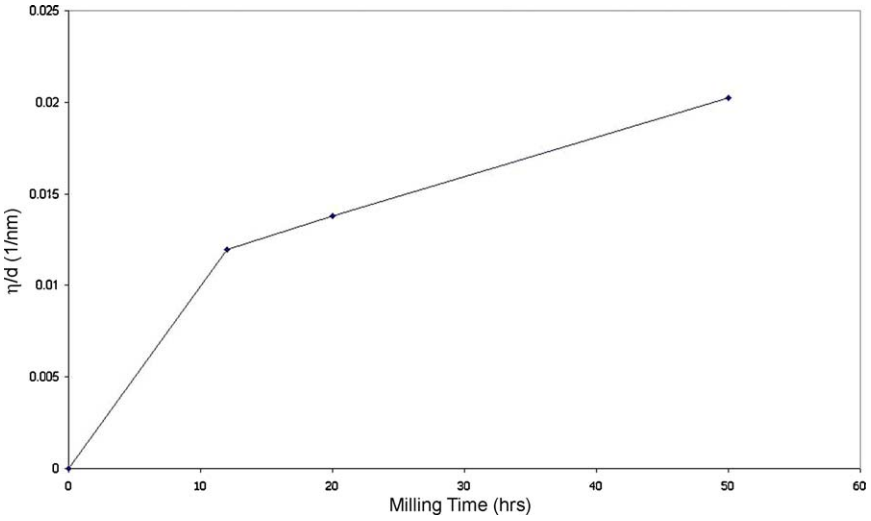

Fig. 3. The effect of the milling time on the mechanical activation parameter of ilmenite.

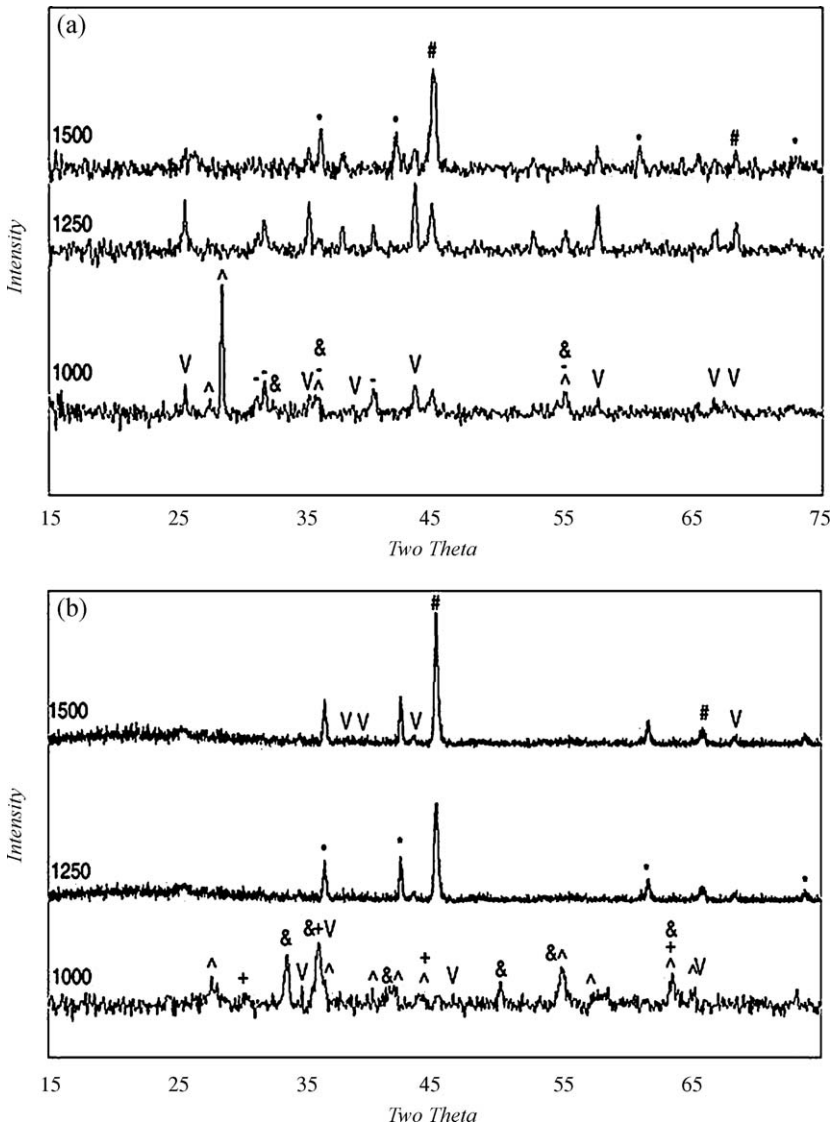

Fig. 4. The XRD pattern of the heat treated samples in $FeTiO_3$–C–Al system: (a) without milling and (b) after 50 h of milling. TiC (*), Al_2O_3 (V), TiO_2 (^), Al_4C_3 (-), Fe (#), Fe_2O_3 (&) and Fe_3O_4 (+).

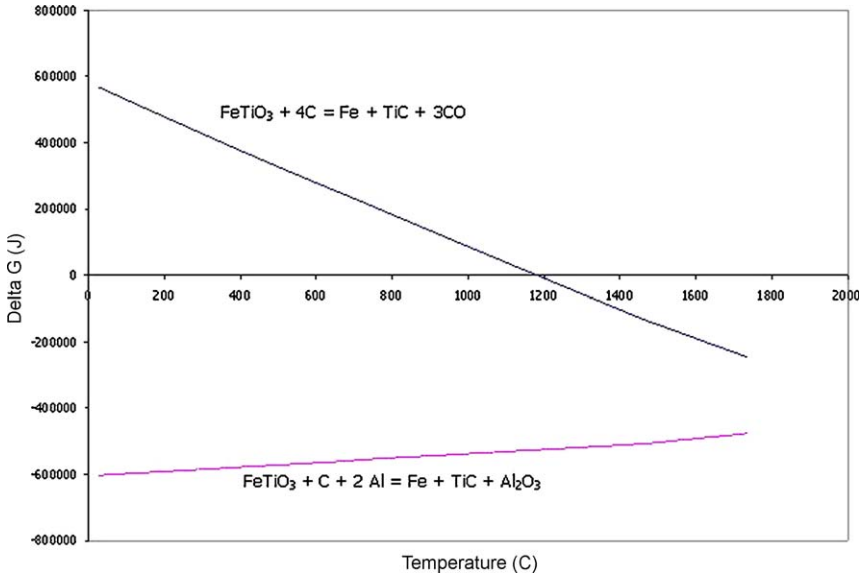

Fig. 5. Ellingham–Richardson diagram of the formation of TiC and Fe from $FeTiO_3$ with or without Al.

increased, the energy of milling is consumed for fining the crystallites and increasing the strain in the system. Consequently, η/d can be identified as a parameter of the mechanical activation of materials. With the use of this parameter, one can predict the kinetic behavior of the milled materials such as the reaction temperature [15]. In Fig. 3, η/d is plotted as a function of the milling time. As shown, increasing the milling time caused in more activation of the materials. This behavior is in accordance with the calculations using Ohlberg and Strickler equation.

Fig. 4 illustrates the XRD patterns of the samples without milling and milled for 50 h after heat treatment. As for the non-milled sample, at 1000 °C, the main phase is TiO_2, which is observed along with Al_2O_3 and Fe_2O_3. Also there are some peaks of Fe and Al_4C_3. As the temperature ascended to 1250 °C, TiO_2 disappeared and TiC peaks appeared slightly. The other phases still remained. As the temperature increased to 1500 °C, the main phases were Fe and TiC. There were also weak peaks of aluminum and iron oxide. Therefore, the formation temperature of TiC was 1000–1250 °C, which has been decreased in contrast to the formation temperature in $FeTiO_3$–C system [22]. This can be attributed to the presence of Al and the formation of Al_2O_3 with regards to Ellingham–Richardson diagram illustrated in Fig. 5 and Eq. (4) [24]:

$$FeTiO_3 + C + 2Al = Fe + TiC + Al_2O_3 \quad (4)$$

In the milled samples, at 1000 °C, Al_2O_3, Fe_2O_3, Fe_3O_4 and TiO_2 phases are observed. As the temperature increased to 1250 °C, TiC is formed, where Fe and Al_2O_3 are also observed. Increasing the temperature to 1500 °C did not change the existing phases and only brought about the intensification of Fe peaks. As it is clear in Fig. 5, the thermodynamic formation temperature of Fe and TiC is 1181 °C. Mechanical activation and also the presence of Al decreased synthesis temperature to below 1250 °C which this value is very close to equilibrium synthesis temperature.

Considering the XRD patterns and the chemical analysis of input materials, the amount of synthesized materials can be determined [25]. The amount of Fe, TiC, Al_2O_3 and other phases were listed in Table 3. From this table, it seems that by increasing the milling time and temperature of heat treatment, the amounts of desirable phases (Fe, TiC and Al_2O_3) were increased. In order to determination of residual aluminum, samples were washed by NaOH and then analyzed by ICP. Furthermore amount of residual carbon was estimated by combustion methods. The amount of free carbon and aluminum in samples were negligible that shows the reactions were completed approximately (Table 3).

In Fig. 2, Williamson–Hall diagram is illustrated for the calculation of crystallite size and the strain in the system. The size of the TiC crystallites produced in this system after

Table 3
The amount of synthesized and residual phases and relative density.

Milling time (h)	Temperature of heat treatment (°C)	Weight percent of synthesized phases based on X-ray diffraction pattern				Weight percent of residual phases measured by ICP		Relative density (%)
		Fe	TiC	Al_2O_3	Other	Free carbon	Free aluminum	
0	1500	36.85	37.35	19.12	6.65	0.04	0.06	92.1
50	1250	37.96	40.03	22.01	–	0.03	0.06	98.7
50	1500	38.14	39.78	22.08	–	0.01	0.02	99.5

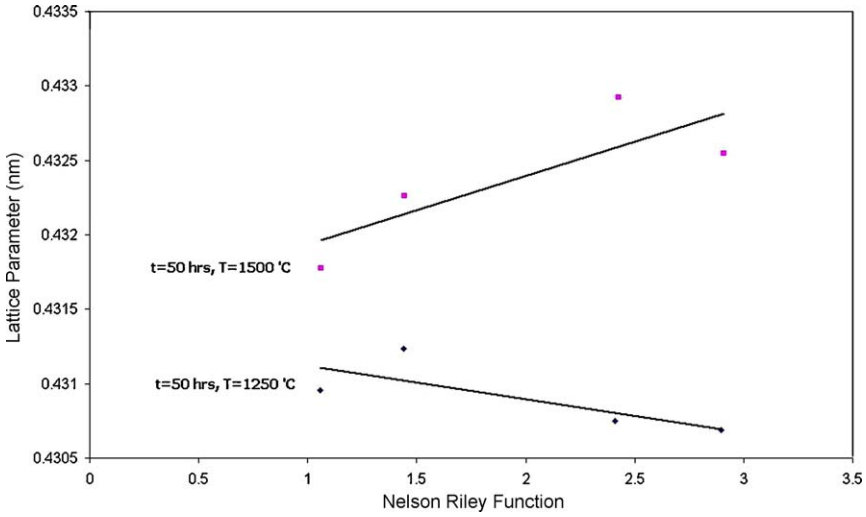

Fig. 6. Nelson–Riley function diagram of the 50 h milled and subsequently heat treated samples.

heat treatment was in the scale of nanometers (Table 2). Therefore, similar to the previous system, a ferrous composite including nanosized reinforcing phase was synthesized. Also from Table 3, it is obvious that sintering and density of samples were intensified by decreasing of crystallite size. This is consistent with the work of other researchers [26].

To determine the lattice parameter of the produced TiC, Nelson–Riley method was utilized. The diagram of the mentioned function is illustrated in Fig. 6. By means of interpolation from the diagram, the lattice parameters of the produced TiC were 0.4313 and 0.4315 nm at 1250 and 1500 °C, respectively. Accordingly, the deviation of the lattice parameter from the ideal size was 0.0014 and 0.0012 nm. As it was expected, this deviation from the standard value reduced as the heat treatment temperature increased. Additionally, there could be further factors causing deviation, such as not calibrating the XRD instrument or not following the exact stoichiometric ratio of the TiC [27].

4. Conclusion

Fe–TiC–Al_2O_3 hybrid nanocomposite was successfully synthesized from ilmenite concentrate, carbon black and aluminum powder. The results showed that increasing the milling time causes the materials to become more active as well as increasing the amorphous phase. Despite heat treatment, the crystallite sizes of TiC were in the scale of nanometers. The crystallite sizes also increased as the heat treatment temperature ascended. Milling process increased the deviation of the lattice parameter from the standard value. However, the deviation decreased as the heat treatment temperature increased.

References

[1] M. Abdel Aziz, T.S. Mahmoud, A. Abdel Aal, Modeling and optimizing of factors affecting erosion–corrosion of AA6063–(TiC/Al_2O_3) hybrid composites by experimental design method, Materials Science and Engineering A 486 (2008) 313–320.

[2] S.K. Thakur, T.S. Kong, M. Gupta, Microwave synthesis and characterization of metastable (Al/Ti) and hybrid (Al/Ti + SiC) composites, Materials Science and Engineering A 452–453 (2007) 61–69.

[3] Q.C. Jiang, B.X. Ma, H.Y. Wang, Y. Wang, Y.P. Dong, Fabrication of steel matrix composites locally reinforced with in situ TiB_2–TiC particulates using self-propagating high-temperature synthesis reaction of Al–Ti–B4C system during casting, Composites: Part A 37 (2006) 133–138.

[4] Z.F. Yang, W.J. Lu, D. Xu, J.N. Qin, D. Zhang, In situ synthesis of hybrid and multiple-dimensioned titanium matrix composites, Journal of Alloys and Compounds 419 (2006) 76–80.

[5] D. Jun, L. Yaohui, Y. Sirong, D. Handa, Effect of fibre-orientation on friction and wear properties of Al_2O_3 and carbon short fibres reinforced AlSi12CuMgNi hybrid composites, Wear 254 (2003) 164–172.

[6] A.K. Mondal, S. Kumar, Dry sliding wear behaviour of magnesium alloy based hybrid composites in the longitudinal direction, Wear 267 (2009) 458–466.

[7] Y.C. Feng, L. Geng, P.Q. Zheng, Z.Z. Zheng, G.S. Wang, Fabrication and characteristic of Al-based hybrid composite reinforced with tungsten oxide particle and aluminum borate whisker by squeeze casting, Materials and Design 29 (2008) 2023–2026.

[8] L. Tong, R.G. Reddy, Synthesis of titanium carbide nano-powders by thermal plasma, Scripta Materialia 52 (2005) 1253–1258.

[9] W.M. Tang, Z.X. Zheng, W.C. Wu, J. Lü, J.W. Liu, J.M. Wang, Structural evolutions of mechanically alloyed and heat treated $Ti_{50}C_{50}$ and $Ti_{33}B_{67}$ powders, Materials Chemistry and Physics 99 (2006) 144–149.

[10] Y.-L. Li, T. Ishigaki, Incongruent vaporization of titanium carbide in thermal plasma, Materials Science and Engineering A 345 (2003) 301–308.

[11] C.J. Lu, Z.Q. Li, Structural evolution of the Ti–Si–C system during mechanical alloying, Journal of Alloys and Compounds 395 (2005) 88–92.

[12] B. Li, Y. Liu, J. Li, H. Cao, L. He, Effect of sintering process on the microstructures and properties of in situ TiB_2–TiC reinforced steel matrix composites produced by spark plasma sintering, Journal of Materials Processing Technology (2009).

[13] D.P. Xiang, Y. Liu, M.J. Tu, Y.Y. Li, W.P. Chen, Synthesis of nano Ti(C,N) powder by mechanical activation and subsequent carbothermal reduction–nitridation reaction, International Journal of Refractory Metals & Hard Materials 27 (2009) 111–114.

[14] S. Singh, M.M. Godkhindi, R.V. Krishnarao, B.S. Murty, Effect of mechanical activation on synthesis of ultrafine Si_3N_4–$MoSi_2$ in situ composites, Materials Science and Engineering A 382 (2004) 321–327.

[15] R. Tahmasebi, M. Shamanian, M.H. Abbasi, M. Panjepour, Effect of iron on mechanical activation and structural evolution of hematite–graphite mixture, Journal of Alloys and Compounds 472 (2009) 334–342.

[16] P. Baláž, Mechanical activation in hydrometallurgy, International Journal of Mineral Processing 72 (2003) 341–354.

[17] C. Sasikumar, S. Srikanth, N.K. Mukhopadhyay, S.P. Mehrotra, Energetics of mechanical activation—application to ilmenite, Minerals Engineering 22 (2009) 572–574.
[18] P. Pourghahramani, E. Forssberg, Effects of mechanical activation on the reduction behavior of hematite concentrate, International Journal of Mineral Processing 82 (2007) 96–105.
[19] V.P. Pavlović, D. Popović, J. Krstić, J. Docilović, B. Babić, V.B. Pavlović, Influence of mechanical activation on the structure of ultrafine $BaTiO_3$ powders, Journal of Alloys and Compounds 486 (2009) 633–639.
[20] M. Razavi, M.R. Rahimipour, T. Ebadzadeh, S.S. Razavi Tousi, Syntheses of Fe–TiC nanocomposite from ilmenite concentrate via microwave heating, Bulletin of Materials Science 32 (2009) 155–160.
[21] M.R. Rahimipour, M. Razavi, M.S. Yaghmaee, Synthesis of TiC–Al_2O_3 nanocomposite from impure TiO_2 by mechanical activated sintering, IJE 21 (2008) 275–280.
[22] M. Razavi, M.R. Rahimipour, Effect of mechanical activation on syntheses temperature of TiC reinforced iron-based nano-composite from ilmenite concentrate, Ceramics International 35 (2009) 3529–3532.
[23] S.M. Ohlberg, D.W. Strickler, Determination of percent crystallinity of partly devitrified glass by X-ray diffraction, Journal of American Ceramic Society 45 (1962) 170–171.
[24] D.R. Gaskell, Introduction to Metallurgical Thermodynamics of Materials, 3rd ed., Taylor & Francis Publisher, 1995.
[25] B.D. Cullity, Elements of X-ray Diffraction, 2nd ed., Addison-Wesley Publisher, 1978.
[26] G.R. Goren-Muginstein, S. Berger, A. Rosen, Sintering study of nanocrystalline tungsten carbide powders, Nanostructured Materials 10 (1998) 795–804.
[27] M. Razavi, M.R. Rahimipour, A.H. Rajabi-Zamani, Effect of nanocrystalline TiC powder addition on the hardness and wear resistance of cast iron, Materials Science and Engineering A 454–455 (2007) 144–147.